Medium-range order in silicon oxycarbide glass by fluctuation electron microscopy

2007 J. Phys.: Condens. Matter 19 455205

(http://iopscience.iop.org/0953-8984/19/45/455205)

IOP PUBLISHING JOURNAL OF PHYSICS: CONDENSED MATTER

J. Phys.: Condens. Matter **19** (2007) 455205 (12pp) doi:10.1088/0953-8984/19/45/455205

Medium-range order in silicon oxycarbide glass by fluctuation electron microscopy

Joseph V Ryan[1] **and Carlo G Pantano**

Department of Materials Science and Engineering, Materials Research Institute, 103 MRI Building, Pennsylvania State University, University Park, PA 16802, USA

Received 14 September 2007
Published 24 October 2007
Online at stacks.iop.org/JPhysCM/19/455205

Abstract

Silicon oxycarbide is a metastable material that has generated interest because of the great flexibility in properties that is attainable with a mixture of divalent and tetravalent anions within the network structure. In addition to the network bonding, however, these materials have also exhibited a strong propensity to include carbon–carbon bonding—so-called 'free carbon'—within the structure regardless of synthesis method. While evidence for the presence of free carbon is overwhelming, traditional diffraction characterization methods have been unable to definitively identify ordering or segregation in the material. Fluctuation electron microscopy (FEM) is a relatively new transmission electron microscopy technique that is specifically sensitive to medium-range order, which is ordered bonding on the length scale of roughly 8–50 Å. We utilize this method to identify semi-ordered bonding present in silicon oxycarbide thin films deposited by reactive rf sputtering over a wide composition range. These results indicate that the use of FEM can be extended to materials which are compositionally heterogeneous at the nano-scale. We show evidence of clusters approximately 1.8 nm in diameter that exhibit correlations similar to the bonding in turbostratic carbon.

(Some figures in this article are in colour only in the electronic version)

1. Introduction and background on silicon oxycarbide

Silicon oxycarbide glasses are being extensively studied as a new class of material with a wide range of property values available through changes in the three-component composition. This versatility is due to the ability to mix high and low valence anions in the glass network, which allows liberal changes in the overall bond density. Several properties (including overall band gap) scale well using a simple bond-mixture model, including density, mechanical properties, optical band gap, and refractive index [1–5].

[1] Present address: Pacific Northwest National Laboratory, Richland, WA 99354, USA.

0953-8984/07/455205+12$30.00

The defining structural unit of silicon oxycarbide consists of a silicon atom tetrahedrally bonded to both carbon and oxygen atoms, denoted by $[SiO_xC_{4-x}]$ with $x = 1, 2$, or 3. Many synthesis techniques have been used to produce materials with a significant fraction of these mixed-anion tetrahedral units, with varying degrees of success [3, 4, 6, 7]. One ubiquitous complication that has been encountered is the formation of carbon–carbon bonding—so-called 'free carbon'—in the glass. Evidence from compositional analysis, electron energy loss spectroscopy (EELS), and Raman studies [3, 7, 8] shows that carbon–carbon bonding is prevalent in these materials. Certain anomalous property observations have been attributed to the presence of this phase, such as better than expected high-temperature stability [9–11] and extremely high resistance to creep [12, 13].

Despite the evidence for the presence of free carbon, it has proven extremely elusive to fully characterize. Bulk silicon oxycarbide materials (polymer-derived ceramics) which have been treated at temperatures over 1200 °C exhibit phase separation of SiC and SiO_2, as well as turbostratic carbon [14]. Extensive TEM analysis on amorphous materials, however, has not been able to directly image a separate phase, suggesting that any segregated volume is both amorphous and extremely small [8, 15, 16]. Even energy-filtered scattering analysis of silicon oxycarbide materials has shown only limited segregation of carbon within the structure of the material [15, 17]. It was initially proposed that the carbon–carbon bonding takes the form of roughly spherical nano-domains or dispersed graphene sheet segments [18, 19], but recently a model ascribing an interconnected net structure to the free carbon phase has been proposed [20] to explain evidence of clustering shown by small-angle x-ray scattering data and observations of high creep resistance [12, 13]. Molecular dynamics investigations of several competing free carbon structural models have not yet yielded a single, unique explanation to account for all available data [21]. In each case, the main complication to direct verification of these models is due to the disordered nature and extremely small size attributed to the domains; each model suggests a characteristic length scale for free carbon of less than 3 nm.

The ability to determine the extent and structure of the free carbon phase is critical for understanding and controlling the engineering properties of this material system. Enhancement and proper dispersion of the free carbon phase can be used to improve the thermal properties and lower the friction coefficient in wear tests [5, 22]. Elimination of the free carbon would likely enable highly scratch resistant optical coatings [1] and allow the synthesis of a variable-refractive-index/optical-band-gap thin film with a single sputtering target [4]. It is necessary to have a detailed understanding of the chemistry and structure of the free carbon in silicon oxycarbides before these materials can be tailored for specific end-uses. Fluctuation electron microscopy (FEM) is a relatively new transmission electron microscopy (TEM) technique that is specifically sensitive to medium-range order (MRO), which is ordered bonding on the length scale of roughly 8–50 Å. We apply this method for the first time on silicon oxycarbide materials in the hopes of uncovering further evidence of ordered structures that could be related to free carbon nano-domains.

2. Background on FEM

FEM, first proposed by Treacy and Gibson [23, 24], is a systematic statistical analysis of dark-field transmission electron microscopy images generated from nominally amorphous materials. Dark-field images are created by electrons that have been coherently scattered by the sample, as opposed to the unscattered (or lightly scattered) electrons in the main beam. Generally, the range of diffraction vectors sampled at any given time, **k**, is controlled by the use of an objective aperture that blocks all other scattering vectors from reaching the detector. Bright areas in

images are produced by electrons from areas of the sample which satisfy the Bragg condition at that particular **k**, while all other electrons, including unscattered electrons, are blocked. In an ideally amorphous sample, the scattering direction is completely random, leading to a random collection of bright and dim areas known as a speckle pattern. In early TEM work, these speckle images were touted to contain extensive real-space information about amorphous structure, but it was later found that similar images could be produced using computer generated random noise [25].

In dark-field imaging, the average intensity of the speckle is due in the first order to the simple atom pair interactions present in the sample. In an amorphous sample, the pair distribution function, $g_2(r, \theta)$, is simply sensitive to the separation distance, r, and is independent with respect to θ due to its isotropic nature. Variable bonding angles and distances present in amorphous samples cause the pair distribution function (and, thus, radial distribution function) of the material to broaden and lose distinction at distances greater than approximately the first three to four nearest neighbors (∼8 Å). In a multicomponent material (such as silicon oxycarbide), this effect is exacerbated by the variations in bond distances between the component pairs, often leading to a loss of information beyond even the second-nearest neighbors [26].

The square of the speckle intensity, however, is governed by higher-order interactions including the $g_4(\mathbf{r}_1, \mathbf{r}_2, \mathbf{r}_3)$ pair–pair distribution function. These interactions are much more sensitive to longer-range order because of the presence of a directionality component in the correlation requirements. Randomly oriented atoms will not meet these stricter requirements and will have only a minor effect on the higher-order distribution function. Small patches of order, on the other hand, will still satisfy the requirements and have a pronounced effect on the high-order distribution function. Theoretical calculations of paracrystalline amorphous silicon models have shown that discrete features can be observed in the $g_4(\mathbf{r}_1, \mathbf{r}_2, \mathbf{r}_3)$ function at distances of five to ten times the nearest-neighbor distance [27], well into the size scale of medium-range order.

While direct measurement of interactions such as the pair–pair correlation has not yet been demonstrated, it is possible to gain insight into these interactions via statistical sampling involving the square of the image intensity. This is done through the analysis of the normalized variance of dark-field images taken at several **k**. The normalized variance, which is a measure of the contrast in the image, is given by

$$V(k) = \frac{\langle I^2(k) \rangle}{\langle I(k) \rangle^2} - 1, \tag{1}$$

where I is the intensity value of each pixel, and $\langle\ \rangle$ denotes averaging over all pixels. Due to the second-order intensity term, the contrast fluctuation in these images is largely a result of higher-order interatomic correlations and therefore is sensitive to the presence of medium-range order. Ordered volumes that are approximately the same size as the resolution limit imposed by the small objective aperture will cause significant increases in the variance compared to a completely random model [28].

3. Experimental procedure

Amorphous silicon oxycarbide films encompassing a wide composition range (figure 1) were deposited by the reactive radio-frequency magnetron sputtering of a carbon-doped SiC target[2] in an atmosphere of mixed oxygen and argon. Fine control of the oxygen-to-argon partial

[2] SG-90, Saint-Gobain.

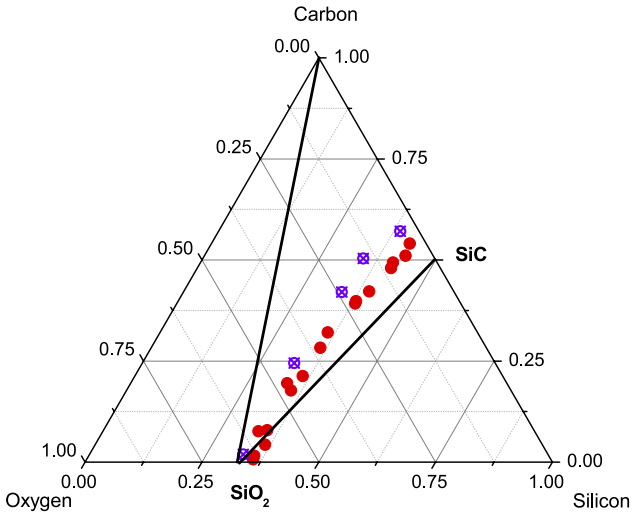

Figure 1. XPS-derived compositions of rf-sputter-deposited silicon oxycarbide thin films. Samples designated with (⊠) were used in this study. The amount of free carbon in the films can be estimated through analysis of compositional deviation from the SiC–SiO_2 pseudo-binary system.

pressure ratio enabled the reproducible synthesis of each desired film composition. Relatively thick films (∼1 μm) were deposited on silicon wafers to determine the deposition rate at each set of conditions. A Taylor-Hobson Talysurf 10 profilometer was used to measure a step-edge created by masking part of the substrate during deposition. FEM samples were then created by depositing ∼70 nm films onto freshly cleaved single-crystal NaCl substrates. Careful control of thickness is important to FEM analysis, especially for a material whose electron scattering characteristics are not well defined. While it is possible to achieve higher variance with a sample ∼20–30 nm in thickness, a thicker sample (∼60–80 nm) generates higher overall dark-field intensity and experiences less sensitivity of the variance response to small changes in thickness [29].

In addition to oxycarbide films, standard films of a-SiO_2 and a-SiC were obtained by the reactive sputtering of a silicon target in oxygen and plasma-enhanced chemical vapor deposition from tetraethylsilane, respectively. All films were transferred onto a 300 square mesh copper grid by dissolving the NaCl substrate in water purified by reverse osmosis. Samples were dried at ambient temperature and no further cleaning or thinning was required. When possible, the sample was analyzed immediately after removal from the deposition chamber, although subsequent measurements on the same samples at a later date showed identical results.

The elemental composition and nominal chemical bonding was studied using high-resolution x-ray photoelectron spectroscopy (XPS) performed on films deposited at the same time as the FEM samples, but onto a silicon wafer section. A KRATOS Axis II Ultra using a monochromatic Al Kα source was used along with locally developed relative sensitivity factors based on Corning 7980 SiO_2, thermally grown SiO_2, polydimethylsilane (PDMS), and single-crystal SiC standards [30]. Oxygen 1s, carbon 1s, and silicon 2p peaks were collected using a 20 eV pass energy, 0.1 eV step, and dwell times of approximately 1000, 4000, and 3500 ms respectively. After this surface scan, the sample was etched for ∼10 s using an argon ion beam in order to remove oxidized surface species and adventitious carbon [31–33]. The current density of the ion etch was such that thermally grown SiO_2 is removed at a rate of ∼1 Å s^{-1}.

High-resolution scans were repeated using the same parameters on this cleaned area and these results were used for compositional analysis. Additionally, extensive characterization on films deposited at the same conditions has been previously reported [34].

All electron microscope images for FEM analysis were collected using a JEOL 2010 TEM with a LaB_6 emitter accelerated at 200 kV and a Gatan Orius™ SC1000 CCD digital camera. Dark and gain normalization procedures were performed regularly to account for any temporal changes to the microscope operation. Though FEM images are improved at low magnification, the objective apertures were brought into sharp focus in diffraction mode, and the sample was then carefully focused in imaging mode and corrected for stigmation at 200 000× magnification or higher to ensure constant sample-beam interactions for each experiment. Shift and tilt purity were also carefully ensured, since the beam tilt is responsible for the abscissa of the variance plot.

The diffraction pattern of the sample was brought into focus and a very small ($\sim$5 μm) objective aperture was inserted to limit the spread of the sampled scattering vectors to ± 0.70 nm^{-1}. The beam was then tilted off-axis so the bright central beam was blocked by the aperture edge and scattered intensity was collected though the aperture in line with the optic axis of the microscope. Dark-field images were first acquired at the smallest diffraction vector allowing complete blocking of the central beam. Subsequent images were taken while increasing **k** stepwise until the signal was too low to produce a reliable image with enough intensity for FEM analysis. Several images were also acquired at wider intervals of **k** after the main data set was completed to check for differences due to beam damage sustained during the experiment. In order to obtain sufficient electron flux at the camera, the sample was imaged at a magnification of 50 000× for all experiments. The extent of tilt was calibrated using polycrystalline NiO_x and Au standards at identical conditions to the analysis. The average number of counts per pixel was kept constant, which necessitated the collection of a prior 'calibration' image at each tilt value to determine the count rate at that specific scattering vector. The entire procedure was repeated at several spots on the same film to decrease the chance of locally anomalous results.

Image analysis was performed using Digital Micrograph software (Gatan, 2006) based on the method detailed by Voyles [29], which entails the following procedure. The modulation transfer function was calculated via the noise method and the shot noise function was calculated from the same data, but once applied, these corrections were not found to appreciably change the variance values. Correct Fourier filtering, however, was critical to the acquisition of consistent and precise data. This step removed the effects of both shot noise and, in some cases, long-range morphological variation. An exclusive disc or ring mask was applied to the Fourier transform of each image. The limit of this filter was chosen manually for each image based on a visual inspection of the information limit of the Fourier transform and a visual analysis of the resulting inverse transform. A minimum range of length scales between 30 and 300% of the resolution limit were allowed to pass.

To limit the effects of spatial variations possible, even considering the relatively constant thickness and consistent morphology of thin films, each 1002 × 668 pixel acquired image was split into 12 sub-images of 256×256 pixels (with a small amount of overlap). These sub-images were 137 nm square and were quite uniform over the area of the image. This also allowed a specific area of each original image to be excluded from the analysis if it was found to contain a thickness variation or some other inhomogeneity. The Fourier filtering was performed on each sub-image, and the variance was calculated for the image resulting from a subsequent inverse transform. Including the sub-images, this necessitated the processing of over 800 images per spot, per sample. A script was written in the Digital Micrograph language that automated this processing and tabulated the data.

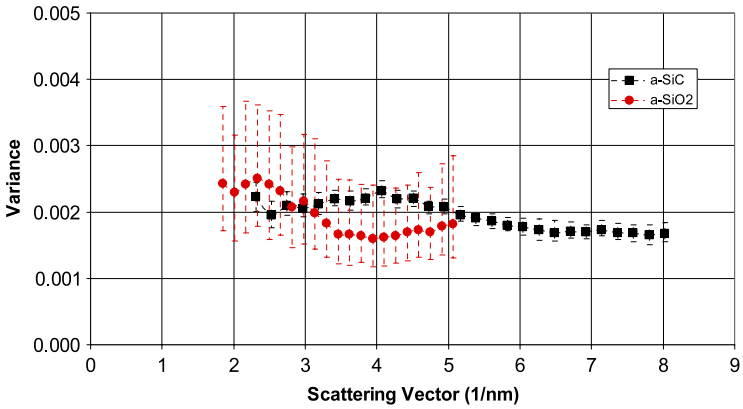

Figure 2. Normalized variance data for a-SiO_2 and a-SiC standard films. The scale is double that used for the silicon oxycarbide data (figures 3 and 4).

4. Results

The XPS-derived elemental compositions (figure 1) show an excess of carbon from a simple $SiO_{(2-2x)}C_x$ stoichiometry where $0 \leqslant x \leqslant 1$. The sample composition would be on the SiO_2–SiC tie-line if every carbon was bonded to four silicon atoms, each oxygen was bonded to two silicon atoms, and every silicon atom was tetrahedrally coordinated with one to four oxygen atoms and the remaining bond(s) to carbon. The deviation from this stoichiometric tie-line in the ternary composition space was used to calculate the amount of carbon in excess of a silicon oxycarbide stoichiometry. Each sample was found to contain between 18 and 25 at.% excess carbon in the structure except for the highest oxygen content sample, which showed less than 5% excess (although this was nearly the entire amount of carbon in that particular sample). It should be pointed out that these excess carbon amounts are used to generally classify the samples and are merely an estimate of the extent of a free carbon chemical structure. Prior work has shown that other bonding types including Si–H, C–H, Si–Si, and C–O are commonly found in these materials [31, 35–38] and will dramatically affect the results of this method of estimating excess carbon independent of the degree of carbon–carbon bonding present. The presence of hydrogen in particular can dramatically affect the stability of the structure [35, 39, 40].

For the fluctuation electron microscopy results, each set of variance values was normalized to a common background level to account for the fact that the absolute value of the variance can be affected by many factors and relative variance changes are more repeatable. The final variance spectrum for each sample is an average of the background-corrected variance for all analyzed spots, with error bars set at one standard deviation. The data for the standard materials are presented in figure 2 and for the silicon oxycarbide samples in figure 3 (high carbon) and figure 4 (medium/low carbon). The objective aperture used in these experiments had an acceptance limit of 0.9 mrad, which limited the resolution of the technique to 1.76 nm at 200 keV and set the dimension of optimum cluster sensitivity. Any signal indicates the presence of clusters with some degree of order at or near this length scale. The width of the peak generally is a function of the degree of ordering: a narrow peak represents a cluster with more consistent order than a broad peak. Peak height is loosely related to the concentration of cluster units, as well as the strength of the scattering from the cluster being probed. These materials were quite resistant to beam damage, showing no change in variance trends after

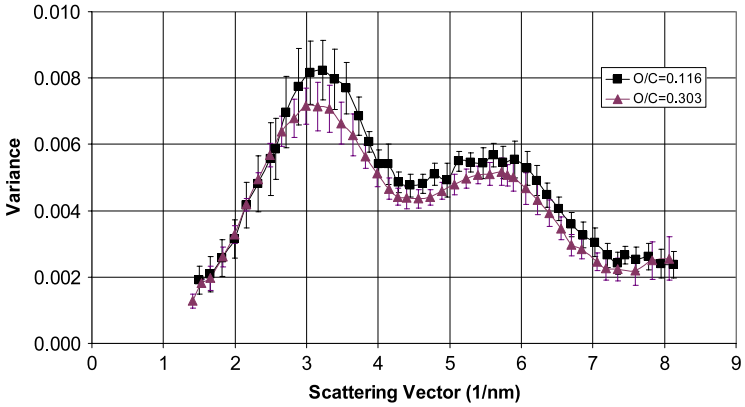

Figure 3. Normalized variance data for silicon oxycarbide samples with O/C $<$ 0.35 (carbon contents over 50 at.%).

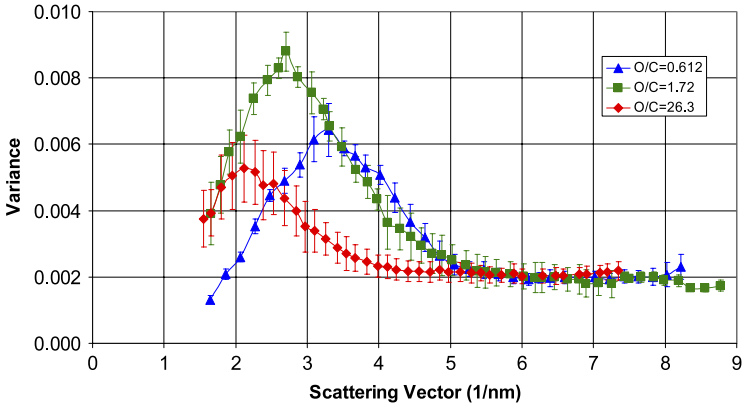

Figure 4. Normalized variance data for silicon oxycarbide samples with O/C $>$ 0.6 (carbon contents less than 26 at.%).

more than 60 min under the beam. There was also no change to the samples visible through a comparison of bright-field images taken before and after the tests.

The reference standards exhibited very little variance overall (figure 2). The variance of a-SiO_2 was almost perfectly flat with changing **k**, with a very small increase in variance observed at $\sim$2.2 nm^{-1}. The a-SiC also showed little change in variance aside from a very broad, minor increase around 4 nm^{-1}. Both samples exhibited variance values approximately an order of magnitude smaller than those of the silicon oxycarbide films.

Figures 3 and 4 show that a maximum in variance at $\sim$3 nm^{-1} is common to nearly all silicon oxycarbide samples. Further, the peak height and width of this first feature is also relatively common, indicating that the films contain roughly the same concentration of this particular type of cluster. One exception is the very low carbon content sample (O/C = 26.6), which had a peak that was shifted to $\sim$2.2 nm^{-1} and was considerably less intense than those of the other three samples. The high-carbon-content samples (O/C = 0.116 and 0.303) included the $\sim$3 nm^{-1} peak, but also exhibited a second peak at $\sim$5.7 nm^{-1}.

5. Discussion

Because fluctuation electron microscopy is fundamentally a diffraction initiated technique, the reciprocal space positions of variance maxima tend to occur at vectors consistent with scattering from crystallographic planes of atoms. In the case of dark-field images of polycrystalline samples, crystallites oriented coincident with a Bragg reflection will appear extremely bright, while crystallites oriented contrary to this direction will not cause strong scattering and thus will be dark. In this case, the overall image contrast is highest at scattering angles that correspond to a Bragg reflection. Indeed, the image contrast is generally very flat outside of the main scattering peaks. This is, in essence, what FEM is measuring. Since the ordered regions in samples studied by FEM generally have fewer correlated atoms, however, a statistical analysis of the normalized variance is necessary to extract useful information.

The particular reference standards used here (a-SiO_2 and a-SiC) were chosen because of the purity of the materials, the well known amorphous nature of the resultant films, and their lack of free carbon. The standards were created as thin films both for ease of comparison with the sample films and to ensure an even-thickness material for TEM analysis. It was assumed that any portion of the sample variance which may be due to amorphized SiC and SiO_2 phases would closely resemble the signal obtained from these standards.

The silicon dioxide film had uniformly low variance over the scattering vector range sampled, indicating very little medium-range order present in the material. The small peak measured at $\sim$2.2 nm^{-1} is at approximately the same position as the |100| peak of low quartz (2.3 nm^{-1}). Most other polymorphs of silicon dioxide also exhibit diffraction at this angle, including high quartz, and both forms of cristobalite [41][3]. The only polymorphs which did not show a reflection at this position (Coesite, Keatite) were high-temperature, high-pressure, or otherwise synthetically produced phases [41] (see footnote 3). It is interesting to note that no signal is observed at $\sim$3.0 nm^{-1}, which is generally the most intense diffraction peak (|101|) for most SiO_2 polymorphs. Amorphous silicon dioxide thin films have been studied previously by FEM [42] and exhibit nearly identical results in terms of the change in variance with **k**, i.e. very low variance with some structure visible at $\sim$2.2 nm^{-1} and no peak observed at $\sim$3.0 nm^{-1}. The results are similar despite the fact that the a-SiO_2 in that study was deposited using chemical vapor deposition rather than sputtering and might be expected to exhibit a different degree of ordering. Evidently, neither of these vapor-deposited amorphous silica films possesses atomic groups correlated similar to |101| planar bonding. These findings may be of assistance in refining the general models for the atomic structure of amorphous silica.

The amorphous silicon carbide film showed a similarly small variance over the full range of scattering vectors. Again, the only noticeable peak (at $\sim$4 nm^{-1}) corresponded well to multiple crystalline polymorphs. In this case, nearly all hexagonal silicon carbide polymorphs (2H, 4H, 6H, 8H, etc) [41] (see footnote 3) have a major reflection at that lattice spacing corresponding to interplanar distances in the *c*-direction. The diamond lattice of the cubic moissanite (α-SiC) polymorph does not have peaks in this range according to x-ray diffraction data, as is also the case with some of the extremely complicated versions of SiC with large unit cell parameters. The presence of variance maxima for the standard materials that align with crystallographic reflections lends credence to the use of FEM to study these types of amorphous solids. Not only was the observed variance small relative to that of the silicon oxycarbide films (indicating much less medium-range order), but the correlation to crystalline versions of each material suggests that the little ordering present is at least in a physically appropriate form.

[3] Joint Committee on Powder Diffraction Standards (JCPDS) Database.

For the silicon oxycarbide films, the variance response of the sample with the lowest carbon content was very similar to that of a-SiO_2 in both shape and position. This film exhibited slightly higher variance than the standard material, but the only peak present was again at $\sim$2.2 nm^{-1}, consistent with the |100| plane of low quartz. As might be expected from the composition of this sample (figure 1), it appears to exhibit the structure of sputtered amorphous silicon dioxide. The little carbon present (2.5 at.%) either did not form ordered regions of free carbon, or was so diffuse that the measurements did not encompass sufficient volume to sample enough ordered free carbon to affect the variance.

The primary features in the samples with total carbon contents over 25 at.% include a broad peak at approximately 3 nm^{-1} and, for samples with total carbon contents exceeding 45 at.%, a second broad peak near 5.5 nm^{-1}. These peaks do not coincide with typical reflections for any of the silicon carbide polymorphs. The peak at 3 nm^{-1} corresponds well to the |101| plane of low quartz, but since this peak is absent from the low-carbon sample, the a-SiO_2 standard, and prior work on a-SiO_2 [42], it is not likely to be due to Si–O bonding. Mixed O–Si–C bonding was considered, but no crystalline oxycarbide phase with this mixed bonding has been reported to date. da Silva *et al* have theorized that a stable SiO_xC_y crystal exists based on *ab initio* molecular dynamics modeling [43], but their structure is based exclusively on a mixture of [SiO_4] and [CO_4] tetrahedra. Experimental data have conclusively shown that mixed silicon oxycarbide tetrahedra are present in these materials [6, 44] and infrared spectroscopy has repeatedly shown very little evidence for C–O bonding in general [37, 45]. Comparisons of the electronegativity and the experimental evidence both suggest that carbon is much more likely to bond to silicon than oxygen in these materials. The peak at 3 nm^{-1}, therefore, is taken to relate to a different structure: that of compositionally homogenous carbon.

The scattering vectors of some planes associated with graphitic bonding seem to match well with the variance data for the higher-carbon-content silicon oxycarbide films. The |002| and |004| planes at 3.0 and 5.8 nm^{-1} respectively correspond to the variance peaks at $\sim$3 and $\sim$5.7 nm^{-1}. The two patterns are not a perfect match, however. The |101| reflection, which is normally the second most intense diffraction peak for graphite, is at 4.95 nm^{-1} and corresponds with a minimum in variance. The fact that this peak is missing helps identify the structure of the possible medium-range order in the sample films.

Graphite exhibits a planar structure, with each plane consisting of hexagonal groups of carbon atoms. In single-crystal graphite, alternating planes are offset from the plane below by half the width of a characteristic hexagonal unit. This periodic offset enables the regular atom spacings that give rise to $|hkl|$ reflections. Disorder introduced into this structure can produce a semi-crystalline polymorph denoted as 'turbostratic' carbon. In this case, the graphene planes are rotated in relation to one another, and the atoms do not exhibit the same repeatable offsets in the *c*-direction. This causes the absence of those reflections caused by interplanar organization, which include any non-zero hk and l combination such as |101|, |111|, etc. Normally, the intraplanar order is undisturbed and the interplanar spacing is relatively unchanged in this material. Therefore, the reflections due to the $|00l|$ planes are still present. Because of the disordered but still evenly layered structure, the name of the material was coined after the Latin *turba* (confused, crowded) and *stratum* (layer) [46]. It is one of the main components of pyrolysis-formed materials such as activated carbons, soot, and coke. Despite the absence of $|hkl|$ reflections, turbostratic carbon does exhibit two-dimensional diffraction due to the regular atomic spacing within the individual planes. The |10| and |11| reflections in particular are hallmarks of this structure [47].

This turbostratic structure appears to be an excellent match to the maxima in variance exhibited by the silicon oxycarbide samples with >45 at.% carbon content. The presence of signal associated with |002| and |004| planes and the lack of signal at 4.95 nm^{-1} (|101|)

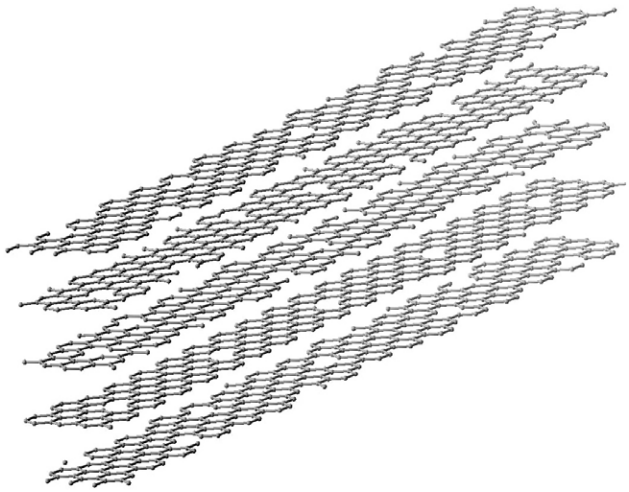

Figure 5. An artist's conception of the disordered turbostratic structure theorized to be exhibited by free carbon in silicon oxycarbide films with high carbon content.

strongly support carbon–carbon bonding correlated in the manner of turbostratic carbon: relatively evenly spaced, but misaligned graphene sheets (figure 5). The fact that the two-dimensional reflections are missing suggests that the individual layers in the structure are themselves quite disordered. The presence of odd-number rings, strained bonds, or vacancies would all diminish the two-dimensional reflections. Buckling of the sheets into the third dimension would also decrease the |10| and |11| scattering.

The FEM data for films with carbon contents between ∼20 and 45 at.% also suggest medium-range order consisting of carbon–carbon bonding. Combining the significance of a variance maximum correlating reasonably well with the |002| reflection of turbostratic carbon with the conclusions derived for the higher-carbon-content samples, it is proposed that correlations similar to those exhibited in turbostratic carbons are present in these films as well. The lack of a |004| peak can be explained by the idea that less exact interplanar correlations exist in the medium-carbon-content samples. Thus, the medium-carbon-content samples exhibit planar bonding that is similar in structure to that of the high-carbon-content films, but is more disordered between planes.

6. Conclusions

The results of this study illustrate that the fluctuation electron microscopy technique is applicable to discerning ordered phase separation on the medium-range order scale (8–50 Å). The differences in crystal-like diffraction between possible phases in the material enable identification of the cluster phase and general correlation structure. In the case of silicon oxycarbide thin films, distinct evidence is found for medium-range order within the free carbon phase at a size scale of approximately 1.8 nm. These carbon clusters exhibit correlations which are similar in nature to disordered turbostratic carbons. This agrees well with published Raman and SAXS data [3, 20, 48] which propose a high degree of sp^2 bonding and 1–2.5 nm clusters respectively. A sister FEM technique known as variable resolution microscopy [27] is currently being applied to these materials to more precisely determine the size of the correlated clusters. Due to the sensitivity of FEM to medium-range order, the formation, evolution, and typical

atomic correlations for ordered carbon structures approximately 1.8 nm in size can be measured within a heterogeneous matrix.

Acknowledgments

Funding was provided by a fellowship through the Penn State Applied Research Laboratory and a grant from the National Science Foundation's International Materials Institute for New Functionality in Glass. All of the characterization in this work was enabled by the Penn State University Materials Research Institute, specifically the Materials Characterization Lab and NanoFabrication Network (NSF Cooperative Agreement No 0335765, National Nanotechnology Infrastructure Network).

Deep thanks are in order to Paul Voyles (University of Wisconsin—Madison), Jing Li (Pennsylvania State University), and Matthew Olszta (Pacific Northwest National Laboratory), whose insights and technical assistance proved invaluable to this project.

References

[1] Wu Q and Gleason K K 2003 *J. Vac. Sci. Technol.* **21** 388–93
[2] Martin-Palma R J, Gago R, Torres-Costa V, Fernandez-Hidalgo P, Kreissig U and Duart J M M 2006 *Thin Solid Films* **515** 2493–6
[3] Pantano C G, Singh A K and Zhang H X 1999 *J. Sol-Gel Sci. Technol.* **14** 7–25
[4] Ryan J V and Pantano C G 2007 *J. Vac. Sci. Technol.* A **25** 153–9
[5] Ryan J V, Columbo P, Howell J A and Pantano C G 2007 in submission
[6] Babonneau F, Bois L and Livage J 1992 *J. Non-Cryst. Solids* **147** 280–4
[7] Soraru G D, Dandrea G, Campostrini R, Babonneau F and Mariotto G 1995 *J. Am. Ceram. Soc.* **78** 379–87
[8] Turquat C, Kleebe H J, Gregori G, Walter S and Soraru G D 2001 *J. Am. Ceram. Soc.* **84** 2189–96
[9] Parmentier J, Soraru G D and Babonneau F 2001 *J. Eur. Ceram. Soc.* **21** 817–24
[10] Soraru G D and Suttor D 1999 *J. Sol-Gel Sci. Technol.* **14** 69–74
[11] Bois L, Maquet J, Babonneau F and Bahloul D 1995 *Chem. Mater.* **7** 975–81
[12] Rouxel T, Soraru G D and Vicens J 2001 *J. Am. Ceram. Soc.* **84** 1052–8
[13] Scarmi A, Soraru G D and Raj R 2005 *J. Non-Cryst. Solids* **351** 2238–43
[14] Soraru G D and Suttor D 1999 *J. Sol-Gel Sci. Technol.* **14** 69–74
[15] Gregori G, Kleebe H J, Blum Y D and Babonneau F 2006 *Int. J. Mater. Res.* **97** 710–20
[16] Kleebe H J, Gregori G, Babonneau F, Blum Y D, MacQueen D B and Masse S 2006 *Int. J. Mater. Res.* **97** 699–709
[17] Gegner J 2003 *Materialwissenschaft und Werkstofftechnik* **34** 290–7
[18] Pantano C G, Singh A K and Zhang H 1999 *J. Sol-Gel Sci. Technol.* **14** 7–25
[19] Brus J, Kolar F, Machovic V and Svitilova J 2001 *J. Non-Cryst. Solids* **289** 62–74
[20] Saha A, Raj R and Williamson D L 2006 *J. Am. Ceram. Soc.* **89** 2188–95
[21] Kroll P 2005 *J. Non-Cryst. Solids* **351** 1121–6
[22] Brequel H, Parmentier J, Walter S, Badheka R, Trimmel G, Masse S, Latournerie J, Dempsey P, Turquat C, Desmartin-Chomel A, Le Neindre-Prum L, Jayasooriya U A, Hourlier D, Kleebe H J, Soraru G D, Enzo S and Babonneau F 2004 *Chem. Mater.* **16** 2585–98
[23] Treacy M M J and Gibson J M 1996 *Acta Crystallogr.* A **52** 212–20
[24] Treacy M M J and Gibson J M 1994 *Ultramicroscopy* **54** 93
[25] Krivanek O L and Howie A 1975 *J. Appl. Crystallogr.* 8 213–9
[26] Varshneya A K 1994 *Fundamentals of Inorganic Glasses* (Alfred, NY: Academic)
[27] Voyles P M, Gibson J M and Treacy M M J 2000 *J. Electron Microsc.* **49** 259–66
[28] Voyles P M and Abelson J R 2003 *Sol. Energy Mater. Sol. Cells* **78** 85–113
[29] Voyles P M 2001 *Thesis* University of Illinois
[30] Shallenberger J R 1996 *J. Vac. Sci. Technol.* A **14** 693–8
[31] Ech-chamikh E, Ameziane E L, Bennouna A, Azizan M, Ngyen T A and Lopez-Rios T 1995 *Thin Solid Films* **259** 18–24
[32] Porte L and Sartre A 1989 *J. Mater. Sci.* **24** 271–5

[33] Seal S, Richardson K A, Lopez C, Graham A, Verma D K, Saliminia A, Galstian T and Villeneuve A 2002 *Phys. Chem. Glasses* **43** 59–65
[34] Ryan J V 2003 *Thesis* Pennsylvania State University
[35] Song S 1999 *Doctoral Thesis* Pennsylvania State University
[36] Gregori G, Kleebe H J, Readey D W and Soraru G D 2006 *J. Am. Ceram. Soc.* **89** 1699–703
[37] Das G, Mariotto G and Quaranta A 2004 *Mater. Sci. Semicond. Process.* **7** 295–300
[38] Brequel H, Soraru G D, Schiffini L and Enzo S 2000 *Metastable, Mechanically Alloyed and Nanocrystalline Materials, Pts 1 and 2* vol 343–3, pp 677–82
[39] Vanek J, Cech V, Prikryl R, Zemek J and Perina V 2004 *Czech. J. Phys.* **54** 937–42
[40] Gracin D, Jaksic M, Bogdanovic-Radovic I, Medunic Z, Car T and Pracek B 2002 *Vacuum* **67** 519–23
[41] Wyckoff R W G 1963 *Crystal Structures* 2nd edn, vol 1 (New York: Wiley)
[42] Ho M Y, Gong H, Wilk G D, Busch B W, Green M L, Voyles P M, Muller D A, Bude M, Lin W H, See A, Loomans M E, Lahiri S K and Raisanen P I 2003 *J. Appl. Phys.* **93** 1477–81
[43] da Silva C R S, Justo J F, Pereyra I and Assali L V C 2005 *Diamond Relat. Mater.* **14** 1142–5
[44] Pampuch R, Ptak W, Jonas S and Stoch J 1979 *Formation of Ternary Si–O–C Phase(s) During Oxidation of SiC* (New York: Elsevier) pp 435–48
[45] Singh A K and Pantano C G 1997 *J. Sol-Gel Sci. Technol.* **8** 371–6
[46] Biscoe J and Warren B E 1942 *J. Appl. Phys.* **13** 364–71
[47] Short M A and Walker P L 1963 *Carbon* **1** 3–9
[48] Flores A, Martos C, Sanchez-Cortes S, Rubio F, Rubio J and Oteo J L 2004 *J. Am. Ceram. Soc.* **87** 2093–100